ADVANCED OPTICAL MATERIALS
www.advopticalmat.de

A Supraparticle-Based Five-Level-Identification Tag That Switches Information Upon Readout

*Franziska Miller, Susanne Wintzheimer, Johannes Prieschl, Volker Strauss, and Karl Mandel**

Product identification tags are of great importance in a globalized world with increasingly complex trading routes and networks. Beyond currently used coding strategies, such as QR codes, higher data density, flexible application as well as miniaturization and readout indication are longed for in the next generation of security tags. In this work, micron-sized supraparticles (SPs) with encoded information (ID) are produced that not only exhibit multiple initially covert identification levels but are also irreversibly marked as "read" upon readout. To achieve this, lanthanide doped CaF_2 nanoparticles are assembled in various quantity-weighted ratios via spray-drying in presence of a broad-spectrum stealth fluorophore (StFl), yielding covert spectrally encoded ID-SPs. Using these as pigments, QR codes, initially dominated by the green fluorescence of the StFl, could be generated. Upon thermal energy input, these particle-based tags irreversibly switch to an activated state revealing not only multiple luminescent colors but also spectral IDs. This strategy provides the next generation of material-based security tags with a high data density and security level that switch information upon readout and can be, therefore, used as seal of quality.

Secure authentication of product components is of great importance in times of constantly growing, non-transparent global trading networks.[1,2] The standard approach is to label macroscopic products with a barcode, which encodes information graphically in 1D and is classified as coding-capacity/identification level 1 (black and white) or 2 (colored) tag.[3] Expanded to 2D, QR-codes have become state-of-the-art, enabling a higher information density (level 3).[4–6] Additional color coding would extend the degree of transportable information even further (level 4, see **Scheme 1**a, left).

F. Miller, Dr. S. Wintzheimer, J. Prieschl, Prof. K. Mandel
Department of Chemistry and Pharmacy
Inorganic Chemistry
Friedrich-Alexander University Erlangen-Nürnberg (FAU)
Egerlandstrasse 1, 91058 Erlangen, Germany
E-mail: karl.mandel@fau.de

Dr. V. Strauss
Max Planck Institute of Colloids and Interfaces
Am Mühlenberg 1, 14476 Potsdam, Germany

Prof. K. Mandel
Fraunhofer Institute for Silicate Research ISC
Neunerplatz 2, 97082 Würzburg, Germany

The ORCID identification number(s) for the author(s) of this article can be found under https://doi.org/10.1002/adom.202001972.

DOI: 10.1002/adom.202001972

Being able to tag an object with a secure but at the same time flexible identification label is an important challenge. Yet, beyond this, it would also be desirable to equip the system with the option of a one-time read-out, i.e., that the tag switches its properties in a clearly visible way once it was readout. A simple, macroscopic, paper-based example of the principle of readout indication has been employed for decades in form of scratchcards (Scheme 1a, right). The scratchcard principle not only has the advantage of readout indication, but quite obviously, it also hides the actual information, which is desired in a number of applications.

All in all, a flexibly applicable tag, carrying protected information of sufficient density due to a higher-level encoding, combines many advantages in one system and enables secure, analogue data storage within materials. However, all macroscopic sticker-based tag solutions are not very flexible in their application due to size restrictions and can be easily counterfeited. For this reason, employing particle-based markers and tracers has been suggested to enable greater flexibility and the possibility to label even smallest product subcomponents and increase the security level.[7–10]

Several approaches have been reported how to generate complex ID patterns using nanomaterials,[11–16] and different levels of security (up to level 4) were claimed.[17–26] Additionally, a luminescent QR code providing a reversible temperature indication has been presented.[27] Yet, the combination of concealing information with a multi-level information pattern introducing a new level 5 of coding-capacity and, on top, a readout indication, has not been reported to date and is demonstrated herein for the first time.

We present a supraparticle (SP)-based pattern, i.e., a label consisting of hierarchically structured, micron-sized entities assembled by nanoparticles, that initially appears as a green luminescent 2D (QR)-code (coding-capacity / identification level 3). To reveal more information, the system has to be activated. This, however, causes an irreversible loss of the green label. Yet, subsequently, under UV light irradiation, it is then possible to either reveal a multicolored spatially resolved code (short-wave UV light, level 4), or a spectral code (long-wave UV light) (Scheme 1b). Thus, this SP-based security tag—beside the combination of readout indication and spatial encoding—provides a spectral ID, expanding its coding-capacity / identification level to a new dimension (level 5).

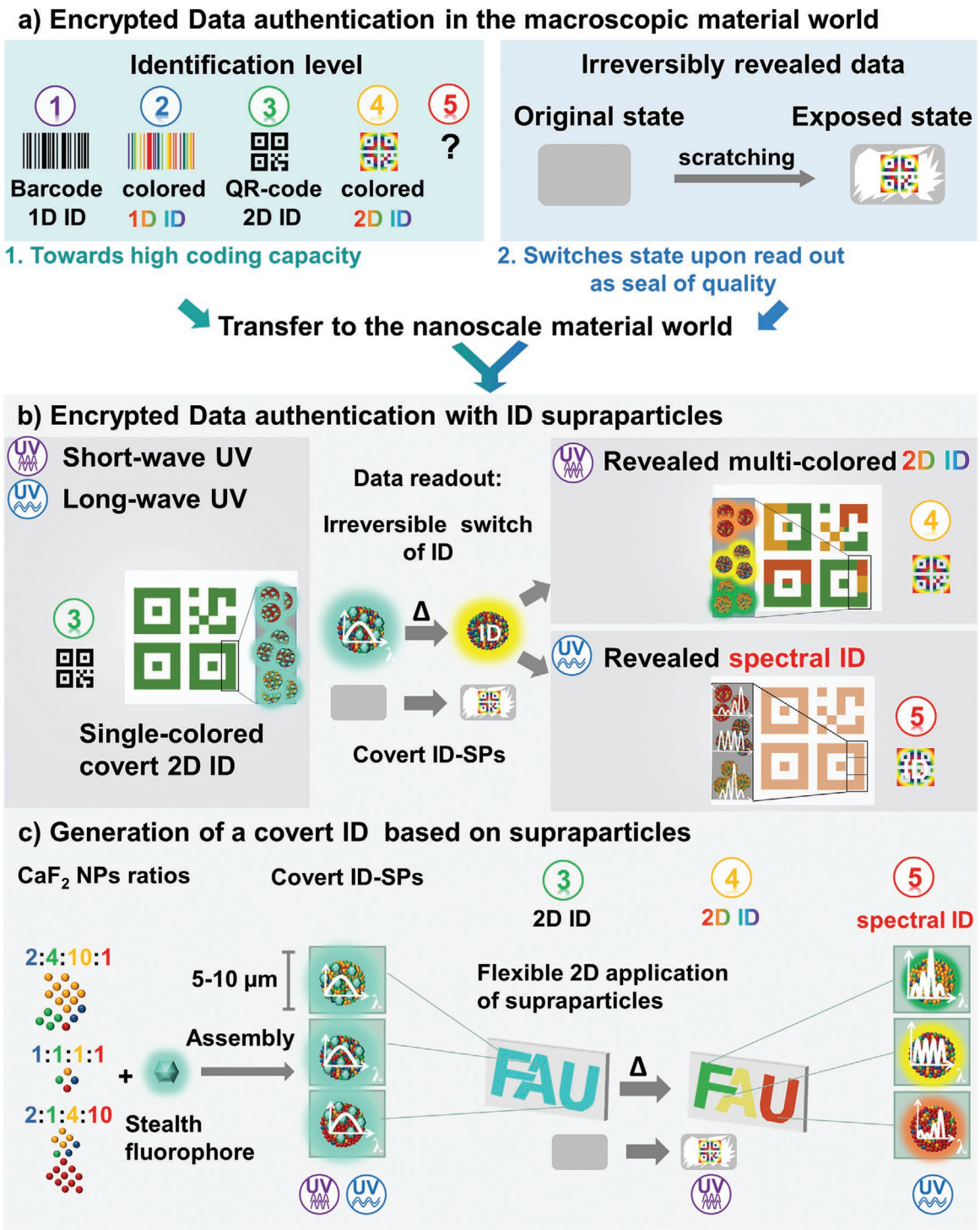

Scheme 1. a) Schematic illustration of the development of spatially resolved marking technologies towards a higher coding capacity (identification levels 1–4) by increasing the dimensionality and chromaticity (left); and with readout indication based on the scratchcard principle (right). b) Schematic depiction of the herein presented approach toward identification and simultaneous readout indication: A single colored ID pattern (identification level 3) is irreversibly switched to an activated state upon thermal energy driven readout, thereby revealing covert information: A previously covert spatial ($\lambda_{exc.}$ = short-wave UV light; identification-level 4) and spectral ($\lambda_{exc.}$ = long-wave UV light; identification level 5) ID can be detected in the activated state of the code. However, this irreversible activation of the code indicates that it was readout and therefore serves as a seal of quality for covert encrypted data. c) Schematic depiction of the development of covert ID codes based on SPs. CaF_2 NPs doped with four different rare-earth ions (Tm^{3+}, Tb^{3+}, Dy^{3+} and Sm^{3+}) are assembled in three defined ratios in the presence of a StFl. After arrangement of the three ID-supraparticle types in a defined pattern (*F A U*), thermal energy input reveals the previously covert spectral and spatial code defined by the rare earth doped SPs luminescence. Due to the irreversible process of StFl decomposition (readout), the code revelation resembles a break of the seal of quality of encrypted data.

Creation of "pigments" for the pattern, in order to achieve the desired system, is the first step: As recently shown, a modular system based on luminescent rare-earth element doped CaF_2 nanoparticles (NPs) (CaF_2:Tm, CaF_2:Tb, CaF_2:Dy and CaF_2:Sm) with unique luminescent properties can be assembled to SPs. These ID-SPs are not only designed to carry a ratiometric code (ID),[28] but they also macroscopically appear in a distinct luminescence color, depending on the ratios of the rare-earth dopants. In order to conceal the information that is inherent to the ID-SPs, the assembly is done in co-presence of broad-wavelength stealth fluorophores (StFl), namely 4-hydroxy-1H-pyrrolo[3,4-c]pyridine-1,3,6(2H,5H)-trione (HPPT). The StFl shows high fluorescence quantum yields of up to 70 % and a broad emission covering a wide range of the visible spectrum.[29,30] Any pattern created with these "pigments" (ID-SPs@StFl) at first appears in a single fluorescence color as the StFl conceals any other spectral information. However, upon thermal energy input (temperature or mid infrared laser irradiation), the StFl decomposes (see Figure S1 in the Supporting Information) and the previously covert ID of the SPs is irreversibly activated both as spatial and as spectral code (Scheme 1c).

Despite the design principle of the overall system appears obvious, on a materials chemistry basis, several challenges arise. This is why, in the following, the advantages of combining all these features within a single SP, and challenges, regarding this approach, are outlined in detail:

- As already described in a preceding work, the principle of ratiometric coding only applies if the coding elements are combined within a single, self-contained, micron-sized SP.[28] This has to be ensured, since it allows a correct readout of the encoded information at any position within the spatially resolved pattern. In the case of simple ratiometric mixture of nanoscale pigments, for example, this is not guaranteed, since the matrix environment might differ among the volume element being analyzed, thus yielding varying signals, making any coding impossible.
- A reliable coverage of the spectral ID is only guaranteed if the StFl is combined with the code-carrying components within the supraparticle units. Only in this case, a separation of the two components can be prevented when these particles are applied in a coating or other matrix material.

Due to these reasons, a supraparticulate architecture had to be designed as a crucial key necessity. As described in detail in a recent review article on SPs,[31] the assembly of several molecular and nanoparticulate building blocks into a SP comes with wanted or sometimes even unwanted emerging phenomena, namely emergence, coupling and colocalization. While properties arising from the structural arrangement of building blocks within a SP (emergence) are not of importance for the herein described system, the interaction of building blocks due to their close contact inside this hierarchically structured microparticle (coupling) and the combination of several properties (colocalization) play important roles. Colocalization is especially aimed for as it provides the before mentioned features of a ratiometric ID, reliable coverage of this ID and homogeneous readout over the entire spatial pattern. For this reason, an important task is to ensure sufficient mechanical stability of the ID-SPs inside the ID tag.

Coupling within the SP is in this case an unwanted phenomenon that appeared in most cases unexpectedly and needed to be circumvented.

Coupling between the StFls, which are pressed together in close proximity within the powdered SPs, could lead to an undesired fluorescence quenching and thus inhibit the system's operating principle. Therefore, a fine adjustment of the StFl concentration and a precise investigation of its influence on the fluorescence properties is crucial.

Further conceivable coupling events could be unfavorable energy transfer processes occurring between the StFls and the ID building blocks prior to their activation, thereby preventing sufficient ID signal coverage.[32–35]

Furthermore, coupling between the ID building blocks and StFl molecules or between the SPs and the surrounding matrix material during the activation could adversely affect the crystallization or diffusion processes taking place during the calcination process, which strongly defines the overall emission ID signature. Consequently unintentional changes in the ID-SPs's optical properties might arise and result in malfunction or destruction of the ID tag.

Even after activation, residues from the StFls that are not completely decomposed could disturb the ID emission signal and thus inhibit its detection.[36,37]

All these challenges were successfully met by the particulate architecture as described in the following.

All syntheses procedures described in the following are provided in exhaustive detail in the supporting information.

To develop the particle system containing a covert ID, rare-earth doped CaF_2 NPs with sizes of ≈30 nm were spray-dried, to form SPs, initially at constant ratio (CaF_2:Tm, CaF_2:Tb, CaF_2:Dy and CaF_2:Sm 1:1:1:1) and the amount of StFl was varied systematically. At any concentration of the StFl, the emission spectra were dominated by the broad fluorescence of the StFl. To ensure that all signals from the ID-SPs were concealed with the StFl fluorescence, the StFl concentration was adjusted to be sufficiently high to cover all other fluorescence signals of the nanoparticles within the SP, but not too high to avoid a fluorescence intensity drop due to concentration-induced quenching. For example, when excited with short-wave UV light, at low StFl concentrations, the emission peak of Tb^{3+} at 541 nm was still detected and at high StFl concentrations quenching due to coupling occurred (**Figure 1**a,c).

To read-out, the ID-SPs@StFl were activated by thermal energy to decompose the StFl. After (thermal / laser) activation, a correlation between the apparent luminescence color of the ID-SPs and the formerly present StFl concentration was observed, namely, with increasing StFl concentrations the luminescence color shifts from green to red. This color change is not due to a classical red-shift, but rather depends on the relative intensity of the Tb^{3+} and Sm^{3+} emission peaks: The higher the StFl concentration, the higher was the Sm^{3+} emission intensity with respect to that of Tb^{3+} when excited with short-wave UV light (Figure 1c,d). This unexpected, yet beneficial coupling effect within the SPs during activation was exploited to obtain the "color hue" yellow by precisely adjusting the StFl concentration (using a concentration of 5 mg StFl per g CaF_2 NPs) in the ID-SPs.

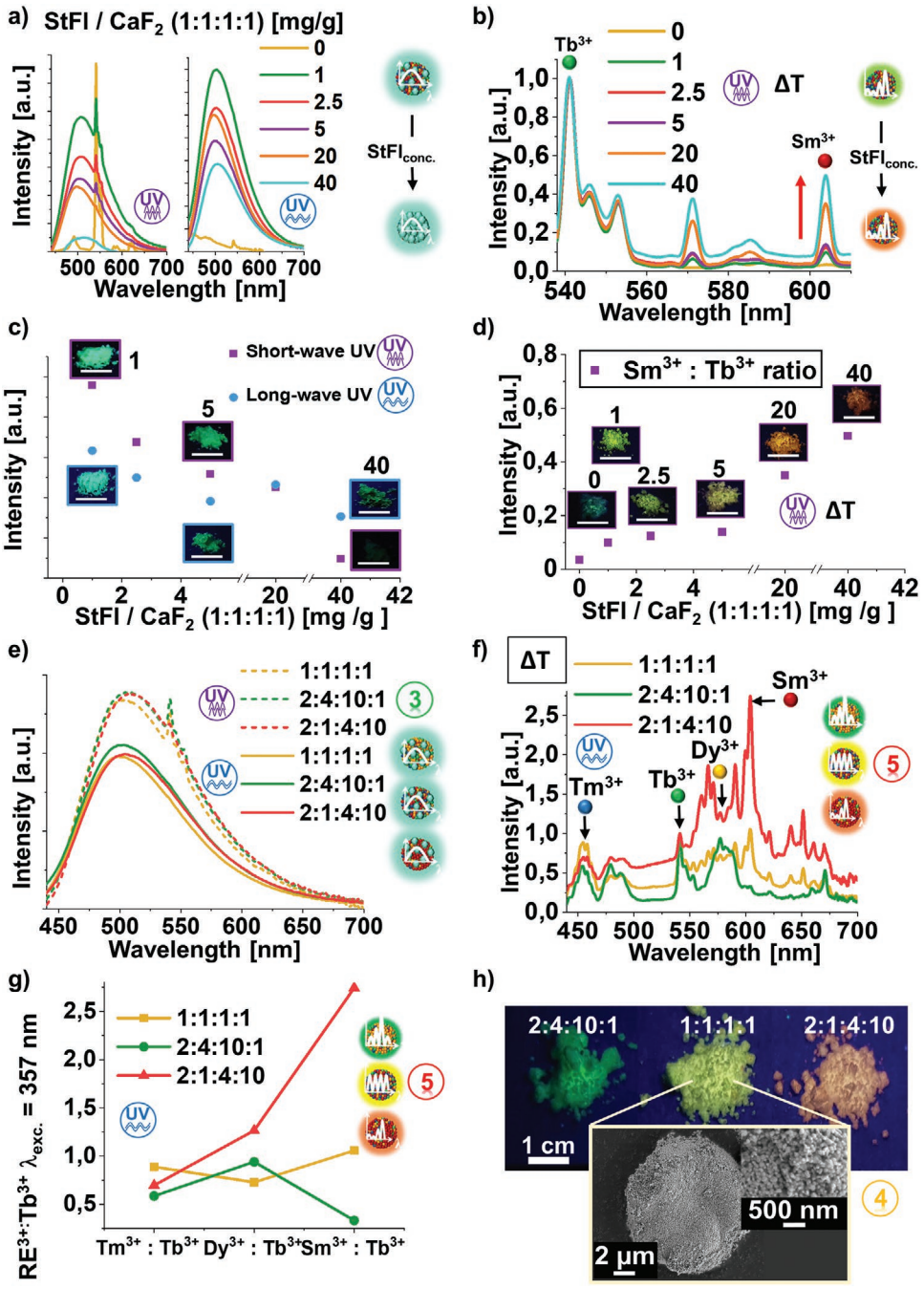

Figure 1. a) Fluorescence spectra of ID-SPs (constant NP ratio: CaF_2:Tm, CaF_2:Tb, CaF_2:Dy and CaF_2:Sm = 1:1:1:1) spray-dried with varying amounts of StFl (left: $\lambda_{exc.}$ = 260 nm, right: $\lambda_{exc.}$ = 357 nm) before and b) after heat treatment (λ_{exc} = 260 nm). c) Graphical display of the emission intensity peaks (at $\lambda_{em.}$ = 507 nm) and the corresponding photographs of the ID-SP powders (scale = 1 cm) irradiated by UV light ($\lambda_{exc.}$ = 254 and 365 nm) and d) after activation ($\lambda_{exc.}$ = 254 nm). e) Fluorescence spectra of ID-SPs (three different NP ratios: CaF_2:Tm, CaF_2:Tb, CaF_2:Dy and CaF_2:Sm = 1:1:1:1, 2:4:10:1 and 2:1:4:10) spray-dried with constant amounts of StFl (5 mg per g CaF_2) before (λ_{exc} = 260 and 357 nm) and f) after activation ($\lambda_{exc.}$ = 357 nm). g) Relative emission intensity ratios of the respective emission peaks of Tm^{3+} (453 nm), Tb^{3+} (542 nm), Dy^{3+} (576 nm) and Sm^{3+} (603 nm) of the three ID-SP-types. h) Photograph of the three ID-SP-type powders irritated by short-wave UV light ($\lambda_{exc.}$ = 254 nm). Inset: SEM image of a thermally treated ID-SP.

TGA results (see Figure S1 in the Supporting Information) indicate that StFl was not fully decomposed when thermally treated. Energy transfer between the rare earth ions and StFl due to coupling might change the probability of f–f electronic transitions and therefore the overall emission signature of the SP.

The apparent fluorescence color of the activated ID-SP is further tuned due to colocalization effects by changing the ratio of rare-earth doped CaF_2 NPs.

Based on the aforementioned findings, three distinguishable ID-SP-types with different rare-earth doped CaF_2

NP ratios (CaF_2:Tm, CaF_2:Tb, CaF_2:Dy, CaF_2:Sm 1:1:1:1, 2:4:10:1, and 2:1:4:10) and the determined ideal concentration of StFl of 5 mg per g CaF_2 were synthesized subsequently and denoted as ID-SPs@StFl. The emission spectra of the three as-prepared ID-SP-types are all covered by the fluorescence of the StFl and cannot be distinguished from one another when excited with long- ($\lambda_{exc.}$ = 357 nm) or short-wave UV light ($\lambda_{exc.}$ = 260 nm). Thus, no spectral ID can be readout initially, since no ratiometry between the rare-earth emission peaks can be deciphered (Figure 1e). Even upon excitation of the ID-SPs@StFl at the excitation maxima of the rare-earth ions, no conclusion about their composition could be drawn, which indicates that the characteristic spectral ID cannot be detected at any excitation wavelength prior to activation, thus proving that the challenging phenomena of fluorophore quenching was successfully circumvented (see Figure S2 in the Supporting Information).

After thermal activation of the ID-SPs@StFl, when excited with short-wave UV light the apparent luminescent colors of the ID-SP-types resemble green (for the 2:4:10:1 system), yellow (for the 1:1:1:1 system) and red (for the 2:1:4:10 system). As mentioned, in all systems, the apparent luminescence colors are mainly determined by the relative Sm^{3+} to Tb^{3+} emission peak ratio (see Figure S3 in Supporting Information for details). When excited with long-wave UV light, the characteristic narrow rare-earth emission bands of all four ID-SP-types were detected (Figure 1f) and their relative emission intensities could be identified (Figure 1g). The three revealed emission ratios resemble distinctive, numerical codes that were previously hidden. Based on findings of a previous study, a single supraparticle, as a self-contained unit, carries the code due to colocalization[28] and thus, in this work, it can be concluded that read out at any position in the QR-code like pattern is possible.

In order to demonstrate the realization of spatially resolved codes, the three different ID-SP-types were incorporated in a thermally stable and transparent SiO_2-based matrix material exemplarily patterned reading "F A U" (see Supporting Information for experimental details). The process parameters were chosen precisely and led to the best optical and yet mechanically stable result. At first, only the single-color-pattern caused by the fluorescence of the StFl is visible (**Figure 2**a,b). Upon exposure to the previously applied temperature treatment (420 °C for 4 h), the fluorophore decomposes, however the characteristic rare earth-based luminescence is not detectable. Rare-earth ion diffusion and CaF_2 crystallization processes which take place during the thermal activation are hindered, probably due to the presence of SiO_2 NPs which act as spatial spacers (see Figure S6 in the Supporting Information). A higher energy input, 620 °C for 10 h results in an adequate revelation of the spatially and spectral resolved previously hidden features without affecting the stability of the coating itself.

Upon short-wave UV light exposure, the different apparent luminescence colors (Figure 2c (top) and Figure S4 in the Supporting Information) become visible. Upon long-wave UV light exposure, no difference in luminescence colors is observed with the bare eye (Figure 2c bottom), but the characteristic rare-earth emission ratios of the three different ID-SP-types at three different spatially resolved positions (F (2:4:10:1), A (1:1:1:1), U (2:1:4:10)) are clearly distinguished spectroscopically (Figure 2d).

To avoid long-term thermal activation, alternatively the readout was accomplished using a commercial laser engraver (experimental section). To this end, films of ID-SPs@StFl were irradiated with a CO_2-laser. The laser energy is absorbed by CaF_2 particles and dissipated in form of heat across the film which leads to an activation of the ID-SPs (see Figure S5 in the Supporting Information).

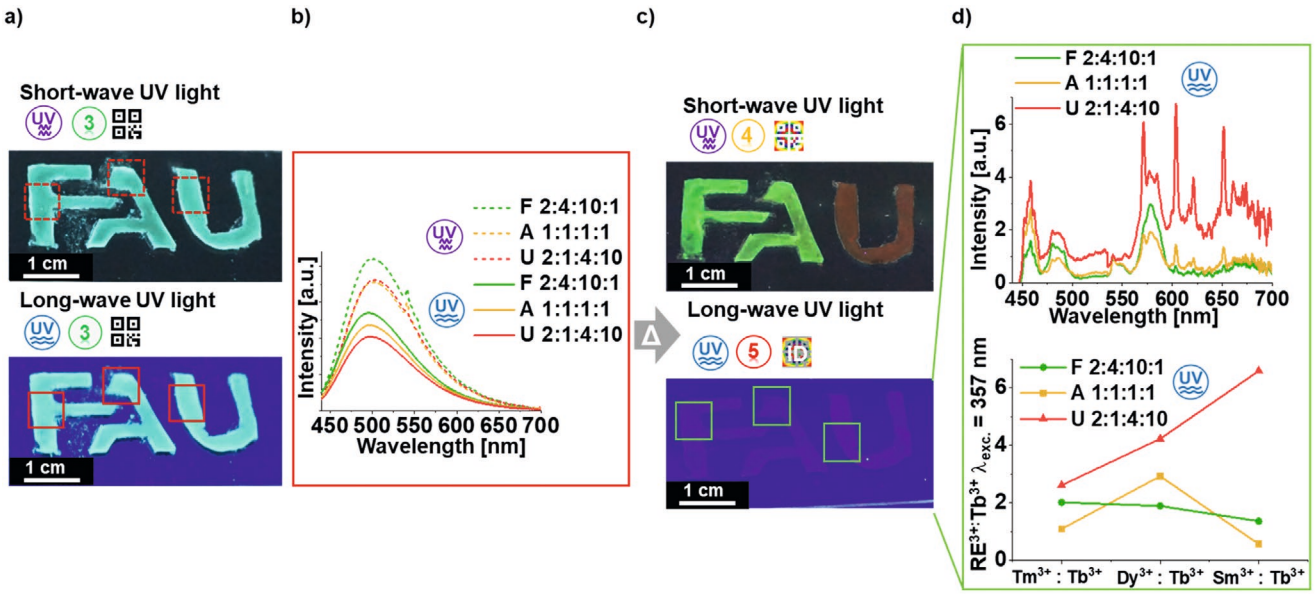

Figure 2. a) Photographs of spatially resolved QR-code like patterns of three ID-SPs@StFl types (*F* = 2:4:10:1, *A* = 1:1:1:1, *U* = 2:1:4:10), $\lambda_{exc.}$ = 254 nm (top) and $\lambda_{exc.}$ = 365 nm (bottom), before thermal activation and b) fluorescent spectra performed at the marked areas ($\lambda_{exc.}$ = 260 nm, dashed curves; $\lambda_{exc.}$ = 357 nm, solid curves) before thermal activation. c) Respective photographs after thermal activation and d) the respective fluorescent spectra after thermal activation for $\lambda_{exc.}$ = 357 nm (top) as well as graphic depiction of relative emission intensity ratios of the respective emission peaks of Tm^{3+} (453 nm), Tb^{3+} (542 nm), Dy^{3+} (576 nm) and Sm^{3+} (603 nm) (bottom).

In summary, micrometer-sized encoded supraparticles (ID-SPs) were produced via spray-drying of luminescent lanthanide doped CaF_2 nanoparticles in the presence of so called stealth fluorophores. By wise selection of the ratios of these building blocks, initially single-colored supraparticles were obtained that contained a covert multicolor spatially resolved ID and a covert spectral ID. More precisely, the spectral code of this organic–inorganic SPs relied on the relative emission intensities of the luminescent nanoparticles. It could be easily modified by changing the concentration ratios of these four different building blocks with distinct optical features. The concealing of the spectral code as well as a characteristic luminescence color was achieved through the stealth fluorophore and its optimal concentration within the supraparticles. Due to their microscale size and powder-form, the supraparticles could be used just like pigments to create single-color fluorescent QR codes. Once this covert code was readout by applying thermal energy, the spatially arranged ID-SPs irreversibly switched to an activated state yielding a coding system combining a distinct multicolor luminescent QR code-like pattern with a spectral ID.

Example scenarios where this is of importance include

i) the ability to verify the "virgin" state of a product or its components, or
ii) the voiding on demand of a product, or
iii) in case of recycling, the simple identification that a component is used for a second time (with potential implications with respect to property and quality degradation).

However, the following limitations of the herein presented system demand further investigation in future: Due to the macroscopic size of the QR code-like ID tag, the advantages of the submicron-sized encoded supraparticles cannot yet be fully exploited. In the future, the focus should therefore lie on miniaturizing the system, thus enabling even the smallest product components to be identified. While the miniaturization of the coding principle is promising thanks to the colocalization property of the supraparticles, adjustments in the detection methodology and signal intensity might be necessary.

Moreover, to ensure a flexible application, further matrix materials for the generation of spatially resolved patterns should be considered as well and evaluated in the future. The implementation of these tags might involve further adjustments regarding the activation process of the ID and the ID SPs nanoparticle composition.

Overall this supraparticle-based approach presents a new generation of security tags providing not only a high data density but also a readout indication and therefore a novel level of security.

Supporting Information

Supporting Information is available from the Wiley Online Library or from the author.

Acknowledgements

This work was financially supported by the BMBF (NanoMatFutur grant 03XP0149), which is gratefully acknowledged. The authors thank BÜCHI Labortechnik AG for providing the spray-dryer equipment. V.S. thankfully acknowledges the financial support from the Max Planck Society and the Fonds der Chemischen Industrie.

Open access funding enabled and organized by Projekt DEAL.

Conflict of Interest

The authors declare no conflict of interest.

Keywords

multilevel luminescence identification, rare earth doped nanoparticles, security tags, stealth fluorophores, supraparticles

Received: November 17, 2020
Revised: December 4, 2020
Published online: December 21, 2020

[1] B. Berman, *Bus. Horiz.* **2008**, *51*, 191.
[2] J. M. Soon, L. Manning, *Food Res. Int.* **2019**, *123*, 135.
[3] E. Schubert, A. Schroeder, *Proc. SPIE* **1996**, *2665*, 59.
[4] W. Berchtold, H. Liu, M. Steinebach, D. Klein, T. Senger, N. Thenee, *Annual Symp. on Electronic Imaging, Science and Technology* **2020**, *7*, 207.
[5] M. Ramya, *Int. J. Comput. Appl.* **2014**, *18*, 8.
[6] N. Taveerad, S. Vongpradhip, in *2015 11th Int. Conf. on Signal-Image Technology & Internet-Based Systems (SITIS)* (Eds: K. Yetongnon, A. Dipanda, R. Chbeir), IEEE, Piscataway, NJ **2015**, p. 645.
[7] D. Paunescu, W. J. Stark, R. N. Grass, *Powder Technol.* **2016**, *291*, 344.
[8] N. H. Finkel, X. Lou, C. Wang, L. He, *Anal. Chem.* **2004**, *76*, 352.
[9] K. Braeckmans, S. C. de Smedt, M. Leblans, R. Pauwels, J. Demeester, *Nat. Rev. Drug Discovery* **2002**, *1*, 447.
[10] S. Shikha, T. Salafi, J. Cheng, Y. Zhang, *Chem. Soc. Rev.* **2017**, *46*, 7054.
[11] Z. C. Kennedy, D. E. Stephenson, J. F. Christ, T. R. Pope, B. W. Arey, C. A. Barrett, M. G. Warner, *J. Mater. Chem. C* **2017**, *5*, 9570.
[12] H. H. Pham, I. Gourevich, J. E. N. Jonkman, E. Kumacheva, *J. Mater. Chem.* **2007**, *17*, 523.
[13] B. Duong, H. Liu, L. Ma, M. Su, *Sci. Rep.* **2014**, *4*, 5170.
[14] Y. Liu, Y. H. Lee, Q. Zhang, Y. Cuia, X. Y. Ling, *J. Mater. Chem. C* **2016**, *4*, 4312.
[15] G. de Cremer, B. F. Sels, J.-I. Hotta, M. B. J. Roeffaers, E. Bartholomeeusen, E. Coutiño-Gonzalez, V. Valtchev, D. E. de Vos, T. Vosch, J. Hofkens, *Adv. Mater.* **2010**, *22*, 957.
[16] J. M. Meruga, A. Baride, W. Cross, J. Kellar, P. S. May, *J. Mater. Chem. C* **2014**, *2*, 2221.
[17] C. Huang, B. Lucas, C. Vervaet, K. Braeckmans, S. van Calenb ergh, I. Karalic, M. Vandewoestyne, D. Deforce, J. Demeester, S. C. de Smedt, *Adv. Mater.* **2010**, *22*, 2657.
[18] Y. Zhang, L. Zhang, R. Deng, J. Tian, Y. Zong, D. Jin, X. Liu, *J. Am. Chem. Soc.* **2014**, *136*, 4893.
[19] S. R. Nicewarner-Peña, A. J. Carado, K. E. Shale, C. D. Keating, *J. Phys. Chem. B* **2003**, *107*, 7360.
[20] P. Kumar, K. Nagpal, B. K. Gupta, *ACS Appl. Mater. Interfaces* **2017**, *9*, 14301.
[21] H. Nam, K. Song, D. Ha, T. Kim, *Sci. Rep.* **2016**, *6*, 30885.
[22] M. You, J. Zhong, Y. Hong, Z. Duan, M. Lin, F. Xu, *Nanoscale* **2015**, *7*, 4423.
[23] H. Liu, M. K. G. Jayakumar, K. Huang, Z. Wang, X. Zheng, H. Ågren, Y. Zhang, *Nanoscale* **2017**, *9*, 1676.

[24] D. Li, L. Tang, J. Wang, X. Liu, Y. Ying, *Adv. Opt. Mater.* **2016**, *4*, 1475.
[25] X. Li, T. Wang, J. Zhang, D. Zhu, X. Zhang, Y. Ning, H. Zhang, B. Yang, *ACS Nano* **2010**, *4*, 4350.
[26] J. F. C. B. Ramalho, S. F. H. Correia, L. Fu, L. M. S. Dias, P. Adão, P. Mateus, R. A. S. Ferreira, P. S. André, *npj Flexible Electron.* **2020**, *4*, 11.
[27] J. F. C. B. Ramalho, S. F. H. Correia, L. Fu, L. L. F. António, C. D. S. Brites, P. S. André, R. A. S. Ferreira, L. D. Carlos, *Adv. Sci.* **2019**, *6*, 1900950.
[28] F. Miller, S. Wintzheimer, T. Reuter, P. Groppe, J. Prieschl, M. Retter, K. Mandel, *ACS Appl. Nano Mater.* **2020**, *3*, 734.
[29] W. Kasprzyk, T. Swiergosz, S. Bednarz, K. Walas, N. V. Bashmakova, D. Bogdał, *Nanoscale* **2018**, *10*, 13889.
[30] V. Strauss, H. Wang, S. Delacroix, M. Ledendecker, P. Wessig, *Chem. Sci.* **2020**, *11*, 8256.
[31] S. Wintzheimer, T. Granath, M. Oppmann, T. Kister, T. Thai, T. Kraus, N. Vogel, K. Mandel, *ACS Nano* **2018**, *12*, 5093.
[32] P. Singhal, B. G. Vats, S. K. Jha, S. Neogy, *ACS Appl. Mater. Interfaces* **2017**, *9*, 20536.
[33] H. Dong, A. Kuzmanoski, D. M. Goßl, R. Popescu, D. Gerthsen, C. Feldmann, *Chem. Commun.* **2014**, *50*, 7503.
[34] F. Hong, Y. Wang, L. Yu, H. Xu, G. Liu, X. Dong, W. Yu, J. Wang, *J. Lumin.* **2020**, *221*, 117072.
[35] T. Samanta, C. Hazra, V. Mahalingam, *New J. Chem.* **2015**, *39*, 106.
[36] J. Panchompoo, L. Aldous, M. I. Wallace, R. G. Compton, *Analyst* **2012**, *137*, 2054.
[37] S. Wintzheimer, J. Reichstein, S. Wenderoth, S. Hasselmann, M. Oppmann, M. T. Seuffert, K. Müller-Buschbaum, K. Mandel, *Adv. Funct. Mater.* **2019**, *29*, 1901193.